Title
EXPERIMENTAL ANALYSIS OF SINTERING OF MgO COMPACTS

Author
Wong, Boon

Publication Date
1978-08-01

Submitted to American Ceramic Society

UC-25
LBL-6294
Preprint

EXPERIMENTAL ANALYSIS OF SINTERING OF MgO COMPACTS

Boon Wong and Joseph A. Pask

August 1978

Prepared for the U. S. Department of Energy
under Contract W-7405-ENG-48

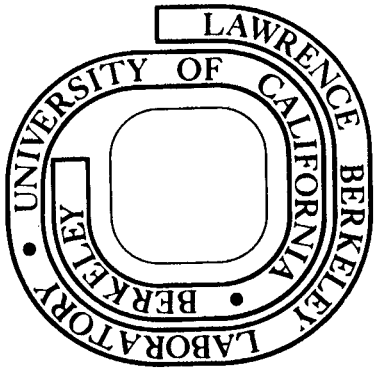

DISCLAIMER

EXPERIMENTAL ANALYSIS OF SINTERING OF MgO COMPACTS

Boon Wong* and Joseph A. Pask

Materials and Molecular Research Division, Lawrence Berkeley Laboratory
and Department of Materials Science and Engineering,
University of California, Berkeley, California 94720

ABSTRACT

Experimental sintering studies on undoped and CaO-doped MgO powder compacts in static air and flowing water vapor atmospheres were performed in the temperature range between 1230°C and 1600°C. Corresponding microstructural changes of specimens during sintering were examined by scanning electron microscopy. Kinetic and microstructural data were analyzed to determine sintering mechanisms during the initial and intermediate stages of sintering.

0

*Based on part of a thesis submitted by Boon Wong for the Ph.D. degree in materials science at the University of California, Berkeley. Now at GTE Laboratories (Sylvania) Waltham, Mass.

I. INTRODUCTION

Previous thermodynamic and geometric considerations[1] of particulate systems densifying by sintering in the absence of a liquid phase indicate that the process can be broadly and ideally divided into two stages: the first in which continuous open pores are maintained, and the second in which only closed pores exist. In real systems, the first stage can be further divided into an initial stage wherein no closed pores form and no grain growth occurs, and an intermediate stage in which some closed pores form and grain growth associated with decrease of number of grains and voids occurs. The second stage practically always shows grain growth and is defined as the final stage of sintering.

The mass transport path causing shrinkage in all instances is movement of material from the grain boundaries forming at grain-grain contacts to the adjoining solid/vapor/solid regions (step 1) and then to the adjoining free surfaces (step 2).[2,3] A further differentiation of the sintering process can be based on whether step 1 or 2 is the slow step. When step 1 is the slow step, essentially no neck forms and the dihedral angle increases continuously during the sintering process until theoretical density or the equilibrium dihedral angle is reached. When step 2 is the slow step, a neck is present whose dihedral angle is continuously and dynamically maintained at the equilibrium value as sintering proceeds. In most systems a neck forms immediately with essentially no shrinkage and has been referred to as the initial stage; in this model, it is referred to as the preliminary stage. An additional complexity is introduced by the observation that rearrangement of particles

frequently occurs during the preliminary, initial and intermediate stages in decreasing severity particularly in compacts of low green or starting density.

It is logical that separate equations would be necessary to represent each stage and case since the nature of the diffusion paths of the controlling step are different and are not constant. Such equations have been derived for the initial and intermediate stages assuming that no rearrangement is occurring.[3] The objective of this paper is to provide experimental verification of these equations by applying them to the data obtained on sintering of MgO powder compacts in static air and flowing water vapor atmospheres, and of CaO-doped MgO compacts in static air.

II. REPORTED SINTERING STUDIES ON MAGNESIUM OXIDE

A number of studies on the sintering of MgO powder compacts and the effect of dopants and atmosphere have been reported. Clark and White[4] obtained densification data which agreed well with their equations for a sintering model based on a viscous or plastic flow mechanism. Brown[5] studied the sintering of very pure magnesia between 1300°C and 1500°C and found that the bulk densities were linearly proportional to $\ell n\ t$ and that the activation energy was 27 Kcal/mole. Reeve and Clare[6] later reanalyzed Brown's sintering data and claimed that the true activation energy for diffusion should be about 79 Kcal/mole which would be in much better agreement with the activation energy for bulk diffusion of Mg in MgO. Nelson and Cutler,[7] Kriek et al.[8] and Layden and McQuarrie[9] concluded that titanium oxide, on the order of 1 mole%, decreased the sintering temperature. Brown[5] showed that sintering was enhanced by vanadium. Also, he found that the densification rate of MgO with 0.01% vanadium followed a t relationship instead of a semi-logorithmic relationship above 1200°C.

Recently, Spencer and Coleman[10] studied the sintering behavior of magnesia along with mixtures containing 0.5 and 1.0 mole% of calcium oxide and forsterite at temperatures between 1400°C and 1800°C. They found that the additions enhanced sintering in the temperature range 1500-1700°C, and increased grain growth was found only for mixtures containing forsterite.

Wermuth and Knapp[11] performed isothermal shrinkage experiments on MgO in dry N_2 and found that shrinkage was proportional to time to

the 0.34 power indicating agreement with a grain boundary diffusion model.

Anderson and Morgan[12] observed a significant acceleration of sintering, as measured by total surface area, by water vapor at pressures lower than 5 mm and at temperatures above the decomposition temperature of $Mg(OH)_2$; the rates were more than 10^3 times faster than in vacuo. They believed that this effect arose from surface diffusion processes induced by adsorbed H_2O. Eastman and Cutler[13] found that water vapor increased the rate of the initial isothermal shrinkage. They concluded that in water vapor atmospheres grain boundary diffusion instead of bulk diffusion was the most probable controlling mechanism, and that the diffusion coefficient was increased by a factor of about 1000 as the partial pressure of water vapor was increased from near 0 to 1 atmosphere. The activation energy for sintering in water vapor at pressures below 5 mm was 80 Kcal/mole and 48 Kcal/mole at pressures above 5 mm.

White[14] also investigated factors affecting the calcination and sintering behavior of magnesia. He showed that crystal growth during calcination or sintering was markedly increased by increasing the partial pressure of water vapor in the flowing air atmosphere and also by increasing the sintering temperature. Most recently, Hoge and Pask[1] examined the sintering of magnesia at 1510°C in three different atmospheres: static air, flowing air, and flowing water vapor, and again showed that the fastest densification rate was in flowing water vapor.

With the range in reported analyses of MgO powder sintering experiments, it seemed worthwhile to undertake this study on the basis of the analysis of the sintering process reported in Ref. (3).

III. EXPERIMENTAL

A. Preparation of Compacts

An analytical reagent grade MgO powder* was calcined at 1100°C in air for 10 hours and then ground in a porcelain mortar with a porcelain pestle to break up the calcined aggregates. After grinding, the powder was dry ball milled with teflon balls in a plastic bottle for 2 hours. The powder was again calcined at 1100°C in air for 10 hours, slightly ground in a mortar, and kept in a vacuum for further use.

The powder for the 0.2 wt% CaO-doped MgO specimens was prepared by mixing the calcined and ground MgO powder with 0.35 wt% analyzed reagent grade $CaCO_3$ powder** in isopropyl alcohol with teflon balls for 10 hours. The powder was then dried in an oven at 110°C, ball milled with teflon balls in a plastic bottle for 2 hours, calcined at 1100°C in air for 10 hours, slightly ground in a mortar, and stored in vacuum for further use. 0.2 wt% CaO is within the solid solubility limits of CaO in MgO in the temperature range studied.

0.5 gm of each powder was loaded in a 0.5 in. diameter steel die, whose walls were lubricated by stearic-isopropyl solution, uniaxially pressed with a pressure of 10 tsi. The green density of each pressed compact was 46% of theoretical; the porosity was thus 54%. At least three specimens were prepared for each sintering run.

---

*Mallinchrodt No. 6015: Loss on ignition 2.0 wt%, MgO after ignition 98.95, Ba 0.005, Sr 0.005, Ca 0.05, Fe 0.01, Mn 0.0005, K 0.005, Na 0.5, Cℓ 0.01, NO_3 0.005, SO_4, 0.015.

**Baker No. 1294: $CaCO_3$ 99.2 wt%, Mg 0.005, Ba 0.002, Sr 0.03, Fe 0.0002, K 0.005, Na 0.008, Cℓ 0.003, SO_4 0.005.

B. Sintering

A bottom-loading type furnace with $MoSi_2$ heating elements was used for the sintering anneals. Isothermal sintering studies were performed in atmospheres of static air and flowing water vapor.

Specimens were distributed on top of a refractory pedestal which was raised into the 1100°C portion of the hot zone of the furnace. For each sintering run, the hottest portion of the hot zone was kept at the sintering temperature. After holding at 1100°C for 1/2 hour, the specimens were raised to the hottest portion quickly and reached the sintering temperature within 20 min. This point was considered zero time. The times at constant temperature ranged from zero minutes to days. After each sintering, the specimens were cooled to 1100°C within 10 minutes by switching off the furnace as well as lowering the pedestal from the hot zone. They were then cooled in air to room temperature. Six sintering temperatures (1280, 1330, 1380, 1430, 1500 and 1600°C) were used for undoped specimens; and two (1330 and 1430°C), for CaO-doped compacts.

For the series of sintering experiments in a flowing water vapor atmosphere, water vapor was introduced into the chamber of the furnace through an alumina tube along the axis of the pedestal. The flow rate of the water vapor was approximately 3.2 liter/min. The water vapor was generated by boiling distilled water in a sealed flask and was carried through hot glass tubing to the alumina tube directly into the furnace. Only undoped MgO compacts were sintered in this atmosphere. All the sintering runs in the flowing water vapor atmosphere had the same heating and cooling cycles as in the static air atmosphere. The flowing water vapor was introduced right after the specimens were raised to the hottest zone of the furnace and cut-off at the end of the isothermal period.

C. Examination of Specimens

The sintered bulk density was determined for each specimen by the ASTM mercury displacement method. The values used for the data analysis for each annealing condition was the averaged density of all specimens subjected to that condition, generally 3 pieces. The total porosity was then calculated on the basis of a theoretical density for MgO of 3.58.

"Fractured," "as annealed," and "polished and subsequently etched" surfaces of selected sintered specimens were coated with about 200 Å gold films and examined with a scanning electron microscope at 300X to 40,000X. The average grain size was determined by the intercept method from the measured lengths of random straight lines drawn directly on the photomicrographs.

IV. EXPERIMENTAL RESULTS AND DISCUSSIONS

Powder preparation and cold compacting procedures received a great deal of attention since the sintering behavior and microstructure of a sintered material are greatly dependent on the homogeneity of the prepared powder and on the uniformity of the density throughout the green compact after cold compacting. An experimental trial and error approach based on optimization was followed to determine the described procedures for powder preparation and cold compacting. With these procedures, no macroscopic chemically bonded aggregates in the powders, no capping or chipping effect on the green compacts, and no macroscopic cracking on sintered pellets were observed. Nevertheless, S.E.M. examinations indicated that even though macroscopic homogeneity existed, microscopic inhomogeneity in the green compacts still persisted.

A. Grain Growth and Microstructural Changes

The grain sizes of several fired specimens of MgO fired at a number of temperatures and times in flowing water vapor and air, and of CaO-doped MgO in air versus their relative densities are shown in Fig. 1. Up to some critical density the grain size is essentially constant and equal to the initial size of about 0.45 microns; densification up to this point is defined as corresponding to the initial stage of sintering. Above the critical relative densities which are approximately 72%, 75% and 80% for the three conditions (corresponding to total porosities of 28, 25, and 20%), grain size increased slowly at first and then rapidly; densification here would correspond to the intermediate and final stages of sintering. In water vapor grain growth occurred at a lower density and the shape of the grain size

curve is different which may be attributed to the contribution to grain growth of a surface diffusion mechanism operating within the compacts which in itself is not contributing to densification.[12] It should be pointed out, however, that the presence of water vapor can also increase the subsurface or bulk diffusivities which make the step (2) mass transport faster and thus contribute to faster densification.

S.E.M. photomicrographs were taken of several typical fracture surfaces of specimens after sintering at 1430°C in static air for various times. Figure 2a shows the microstructure after 30 min at temperature which is still in the initial stage with a fractional porosity of 0.39. A specimen heated for 303 min, with a porosity of 0.14, was in the intermediate stage and had the microstructure shown in Fig. 2b. After 1110 min the specimen had a porosity of 0.09 and was in the final stage of sintering (Fig. 2c); the "as annealed" surface of this specimen is shown in Fig. 2d. It is of interest to note that in the final stage of sintering when closed pores are still revealed on a fractured surface, the "as annealed" surface shows no pores.

An analysis of the grain size and microstructural relationships supports the division of the sintering process into three stages. In the initial stage, essentially no closed pores have formed and no grain growth has occurred. In the intermediate stage, above the critical relative density, some pores are closing and grain growth is occurring, but continuous open pores are still present. In the final stage, only closed pores exist and grain growth occurs rapidly.

In accordance with previous discussions[1-3] the tendency for neck formation and the nature of the dihedral angle formed by the grain

boundary and the two free particle surfaces at grain/grain contacts is a reflection of the rate controlling mass transport mechanism. Two specimens with densities of 81% of theoretical after sintering in static air and flowing water vapor are shown in Figs. 3a and 3b. In static air, necks with large dihedral angles form at triple points, as pointed out by the arrows, under conditions when the rate controlling step is movement of material from the neck regions to the free surfaces. In flowing water vapor, necks did not form as readily due to rapid removal of any developing reverse curvature in the free surfaces and the dihedral angles were thus smaller, as seen in Fig. 3b, representing conditions when the rate controlling step is movement of material along the grain boundary to the neck areas.

Appropriate sintering equations have to be applied to the data for each of the sintering stages. Also, the equation has to take into account the different mass transport controlling mechanism that may exist under a particular experimental condition.

B. Densification Results

Figures 4, 5 and 6 present the porosity versus time data at various temperatures for the undoped MgO compacts in static air and flowing water vapor atmospheres and 0.2 wt% CaO-doped MgO compacts in static air atmosphere, respectively. The heating schedules were described earlier. The porosity at zero time indicates the degree of sintering that had occurred by the time the test temperature was reached; all of the specimens had a starting unfired porosity of 54%. The scatter of data can be attributed to the microscopic inhomogeneities in the green compacts and experimental variations.

In static air atmosphere, for undoped MgO compacts at a given temperature, porosity is linearly proportional to time and the densification rate remains constant up to the critical relative density of about 75% and decreases with increasing time above the critical density (Fig. 4). The CaO-doped MgO compacts behave in a similar manner with a critical relative density of about 80% (Fig. 6). In flowing water vapor atmosphere, the undoped MgO compacts show no constant densification rate periods with increasing time for all temperatures (Fig. 5). A comparison of the curves for 1330°C, for example, indicates that the undoped MgO in static air sinters the slowest and in flowing water vapor, the fastest.

1. Undoped MgO in Static Air Atmosphere

Porosity is proportional to time down to the critical porosity of 25% as seen in Fig. 4. These data suggest that the controlling step for densification in this initial stage is movement of material from the neck areas to the free surfaces. The sintering equation[3] is

$$(P - P_o) = -\frac{A_1 D_B \Omega \gamma_{SV} N^3}{kT} (t - t_o) \qquad (1)$$

where A_1 is a porportionality constant, P is the porosity, t is the sintering time, D_B is the bulk diffusion coefficient, Ω is the atomic (molecular) volume, γ_{SV} is the specific surface free energy at the solid-vapor interface, T is the absolute temperature, k is Boltzmann's constant, P_o and t_o are the initial porosity and time on reaching the test temperature T, and N is the number of interconnected voids per unit volume which remains constant during this stage. N is inversely proportional to G, grain size, which determines the number of grains per unit volume for a given packing.

The decrease in densification rates (Fig. 4) and the commencement of grain growth (Fig. 1) at porosities less than 25% indicates the termination of the initial stage and the beginning of the intermediate stage of sintering. At this point G and N are no longer constant and P is proportional to $\ell n\ (t/t_o)$ as shown in Fig. 7 and the equation becomes

$$(P-P_o) = -\frac{A_1 D_B \Omega \gamma_{SV}}{mkT}\ \ell n\ \frac{t}{t_o} \qquad (2)$$

where A_1 is a proportionality constant and m is the time-independent coefficient in the relationship for the reduction of the number of voids.[3] Limited data show straight line portions between porosities of 25% and ~10% as required by this equation for the intermediate stage.

Sufficient data were not available for an analysis of the final or closed pore stage. The specimens brought up to 1600°C were already in the final stage upon reaching temperature or at zero time. There is also an indication of an end-point porosity of ~0.05 which can be attributed to inhomogeneities introduced in processing and pores entrapped in grains.

Sintering rate coefficients K_1, were determined according to Eq. (1) from the slopes of the linear portions of the curves in Fig. 4 and plotted in Fig. 8 as $\ell n\ K_1$ versus the reciprocal of absolute temperature. The activation energy was determined to be 112 Kcal/mole. This value agrees well with the activation energies for self-diffusion of oxygen ions in MgO single crystal (110±4 Kcal/mole).[15]

The apparent activation energy for the intermediate stage, as seen from the data in Fig. 7, has a low value of opposite sign. This result is considered to be due to two processes taking place concurrently:

grain growth or reduction of voids and densification. There were insufficient data to evaluate the contribution of each of the processes.

2. Undoped MgO in Flowing Water Vapor Atmosphere

When grain boundary diffusion is the controlling mechanism during the initial stage of sintering, dynamic dihedral angles exist at triple lines which increase in size with sintering, and the following kinetic equation applies:[3]

$$\left[\tanh^{-1}(-0.43P^{1/2} + 0.3) - \tanh^{-1}(-0.43\ P_o^{1/2} + 0.3)\right] = \frac{A_3\gamma_{SV}D_{gb}\omega\Omega N^4}{kT}(t - t_o) \qquad (3)$$

where A_3 is a proportionality constant, D_{gb} is the grain boundary diffusion coefficient and ω is grain boundary width. The factor 0.3 is the result of an assumption of 140° as the equilibrium dihedral angle.

Figure 5 shows curves with no straight line portions, but a plot of the data from these curves according to Eq. (3) does show straight lines at porosities greater than the critical value of about 0.28 as seen in Fig. 9. Some other value for the equilibrium dihedral angle will change the factor of 0.3 and shift the positions of the curves, but the slopes of the straight line portions will not change. Even though densification was so rapid in water vapor that the specimens were close to the intermediate stage of sintering by the time they reached the test temperature, the slopes of the linear portions K_2 of Fig. 9 were determined and plotted in Fig. 8. The apparent activation energy value of 50 kcal/mole agrees well with the reported value of 48 kcal/mole for initial sintering of MgO compacts in atmospheres with high water vapor pressures.[13]

With the occurrence of significant normal grain growth and reduction of number of voids per unit volume, which is the initiation of the intermediate stage, Eq. (3) becomes

$$\tanh^{-1}(-0.43\ P^{1/2} + 0.3) - \tanh^{-1}(-0.43\ P_o^{1/2} + 0.3) =$$

$$-\frac{A_4 \gamma_{SV} D_{gb} \omega \Omega}{kTm^{4/3}} \left(\frac{1}{t^{1/3}} - \frac{1}{t_o^{1/3}} \right). \qquad (4)$$

where A_4 is a proportionality constant. Data taken from Fig. 5 and plotted according to Eq. 4 are shown in Fig. 10. Straight line portions were obtained at porosities below the critical value of 0.28. An apparent activation energy was not calculated because of concurrent processes, as before.

3. CaO-Doped MgO in Static Air Atmosphere

Data for the CaO-doped MgO compacts were obtained only at 1330 and 1430°C in static air atmosphere as shown in Fig. 6. A straight line portion exists at 1330°C for porosities greater than 20% suggesting that the rate controlling mass transport mechanism in the initial stage is similar to that for undoped MgO in static air. Sufficient data were not available for activation energy determinations.

V. SUMMARY AND CONCLUSIONS

Sintering behavior of MgO compacts as prepared was found to be sensitive to the nature of the atmosphere and to CaO-doping as reported in the literature. Analysis of microstructural changes and kinetic data supported the distinct existence of initial, intermediate and final stages in the sintering of this powder in accordance with theoretical analysis.[1-3] The latter two stages were identified as exhibiting grain growth and decrease of number of voids per unit volume, and the final stage as one containing no open continuous pores. Previously derived equations[3] were applied to the initial and intermediate stages. In air, porosity was found to be proportional to t in the initial stage and to $\ell n\ t$ in the intermediate stage, both of which are based on the fact that the rate controlling step is the transport of mass from the neck region to the adjoining free surface regions. In flowing water vapor, the porosity function of $\tanh^{-1}\ (-0.43P^{1/2} + 0.3)$ was found to be proportional to t in the initial stage and to $t^{-1/3}$ in the intermediate stage, both of which are based on the fact that the rate controlling step is the transport of mass from the grain/grain contact to the adjoining neck regions during which the length of the diffusion path increased as densification progressed.

The apparent activation energies for the sintering of undoped MgO compacts in static air and flowing water vapor atmospheres in the initial stage were determined to be approximately 112 and 50 Kcal/mole, respectively. The former corresponds to the value for bulk diffusion of oxygen whereas the latter corresponds to the value for grain boundary diffusion which is consistent with the suggested mechanisms. Sufficient

data was not available for determination of the apparent activation energies during the intermediate stage for undoped MgO, and for both stages for CaO-doped MgO compacts.

Experimental data was insufficient to analyze the final stage of sintering. The undoped specimens heated in air appeared to approach an end-point density of about 95% of theoretical and in water vapor, about 91% of theoretical. This occurrence can at least partially be attributed to inhomogeneities in the unfired compact and entrapped gases. There is also the possibility that the $(\gamma_{ss}/\gamma_{sv})_{eq.}$ ratios were generally too high for the degree of packing of the powder to realize theoretical density in the final stage. Any preliminary rearrangement and framework formation was not noted experimentally since, if it occurred, all of the specimens were into at least the initial stage of sintering by the time they reached the isothermal test temperatures.

ACKNOWLEDGMENT

This work was supported by the Division of Materials Sciences, Office of Basic Energy Sciences, U.S. Department of Energy.

REFERENCES

1. C. E. Hoge and J. A. Pask, Thermodynamic and Geometric Considerations of Solid State Sintering, Ceramurgia International, 3 [3], 95-99 (1977).
2. J. A. Pask, C. E. Hoge and B. Wong, Dependence of Sintering Characteristics on Thermodynamic and Geometric Factors, in Ceramic Microstructures, '76, edited by Richard M. Fulrath and Joseph A Pask, Westview Press, Boulder, CO, pp. 246-254, 1976.
3. B. Wong and J. A. Pask, Models for Kinetics of Solid State Sintering, submitted to J. Am. Ceram. Soc.
4. P. Clark and J. White, Some Aspects of Sintering, Trans. Brit. Ceram. Soc., 49, 305 (1950).
5. R. A. Brown, Sintering in Very Pure Magnesium Oxide and Magnesium Oxide Containing Vanadium, Bull, Am. Ceram. Soc., 44 [6], 483 (1965).
6. K. D. Reeve and T. E. Clare, Comments on Papers "Sintering in Very Pure Magnesium Oxide and Magnesium Oxide Containing Vanadium" and "Sintering in Calcium Oxide and Calcium Oxide Containing Shontium," J. Am. Ceram. Soc., 49 [7] 400, (1966).
7. J. W. Nelson and I. B. Cutler, Effect of Oxide Additions on Sintering of Magnesia, J. Am. Ceram. Soc., 41, 406 (1958).
8. H. J. S. Kriek, W. F. Ford and J. White, The Effect of Additions on the Sintering and Dead-burning of Magnesia, Trans. Brit. Ceram. Soc., 58 1, (1959).
9. G. K. Layden and M. C. McQuarrie, Effect of Minor Additions on Sintering of MgO, J. Am. Ceram. Soc., 42 89, (1959).

10. D. R. F. Spencer and D. S. Coleman, Sintering and Crystal Growth of Magnesia in the Presence of Lime and Forsterite, Mineralogical Magazine, 37 [291], 839 (1970).

11. F. R. Wermuth and W. J. Knapp, Initial Sintering of MgO and LiF, Doped MgO, J. Am. Ceram. Soc. 57 [7], 401 (1973).

12. P. J. Anderson and P. L. Morgan, Effect of Water Vapour on Sintering of MgO, Trans. Faraday Soc., 60 [5], 930 (1964).

13. P. F. Eastman and I. B. Cutler, Effect of Water Vapor on Initial Sintering of Magnesia, J. Am. Ceram. Soc. 49 [10], 526 (1966).

14. J. White, Refractories Research II. Calcination and Sintering of Magnesia, J. Australian Ceram. Soc., 9 [2], 60 (1973).

15. J. Narayan and J. Washburn, Self Diffusion in MgO, Acta Met. 21, 533 (1973).

FIGURES

1. Grain size vs. bulk density for MgO compacts in air and flowing water vapor and for CaO-doped MgO compacts in air.
2. Microstructures of fracture surfaces of MgO compacts obtained by SEM after sintering at 1430°C in static air for (a) 30 min (fractional porosity of 0.39), (b) 303 min (0.14), and (c) 1110 min (0.09). The "as annealed" surface of (c) is shown in (d).
3. Microstructures of fracture surfaces of MgO compacts, obtained by SEM, sintered to a density of ~81% of theoretical (a) in static air and (b) in flowing water vapor.
4. Porosity vs. time for MgO compacts sintered in static air.
5. Porosity vs. time for MgO compacts sintered in flowing water vapor.
6. Porosity vs. time for CaO-doped MgO compacts sintered in static air.
7. Porosity vs. $\ell n\ t$ for MgO compacts sintered in static air.
8. Rate constants vs. 1/T for MgO compacts sintered in static air and flowing water vapor during the initial stage.
9. Porosity functions vs. time for MgO compacts sintered in flowing water vapor.
10. Porosity function vs. $t^{-1/3}$ for MgO compacts sintered in flowing water vapor.

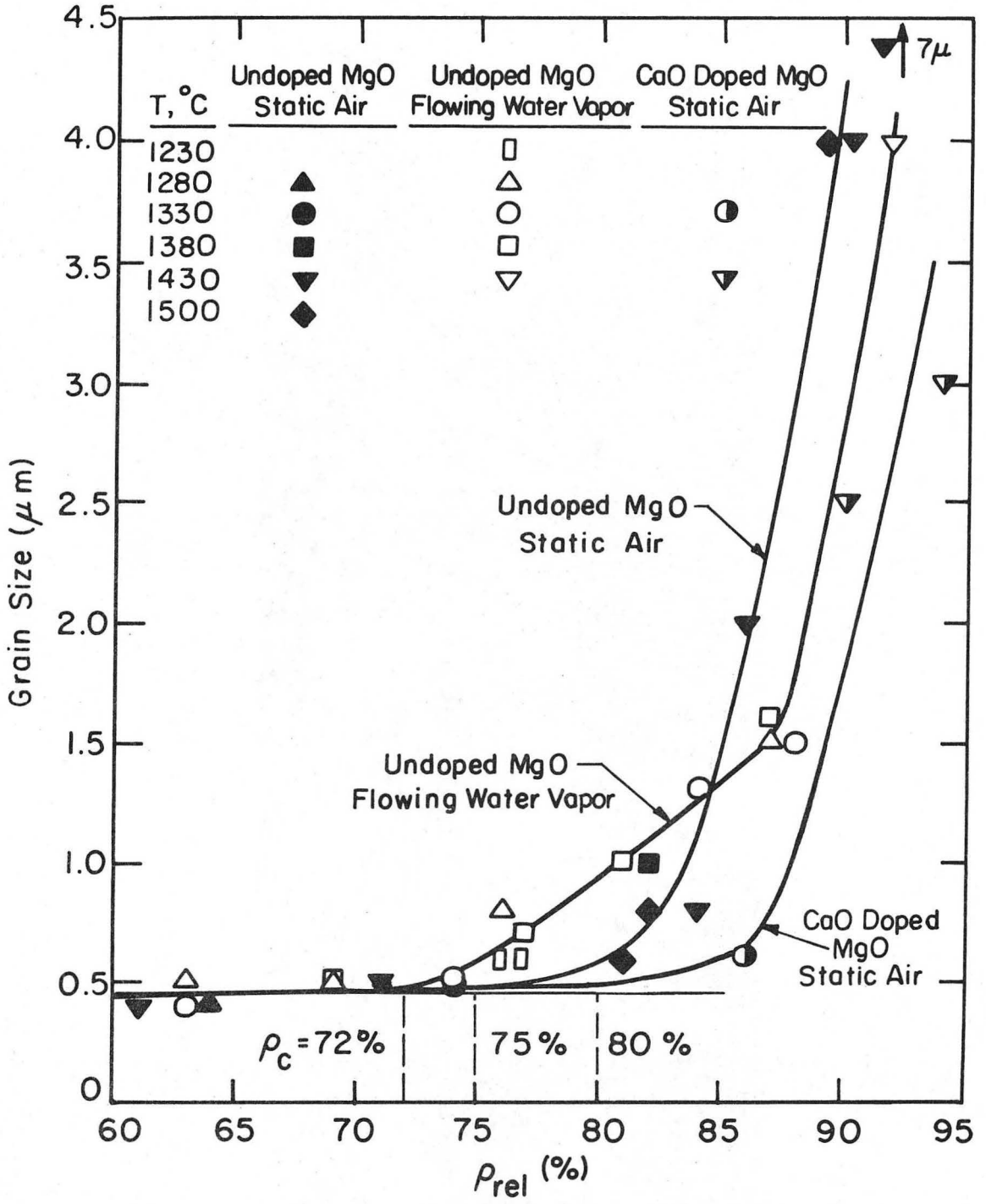

XBL 759-7236A

Fig. 1

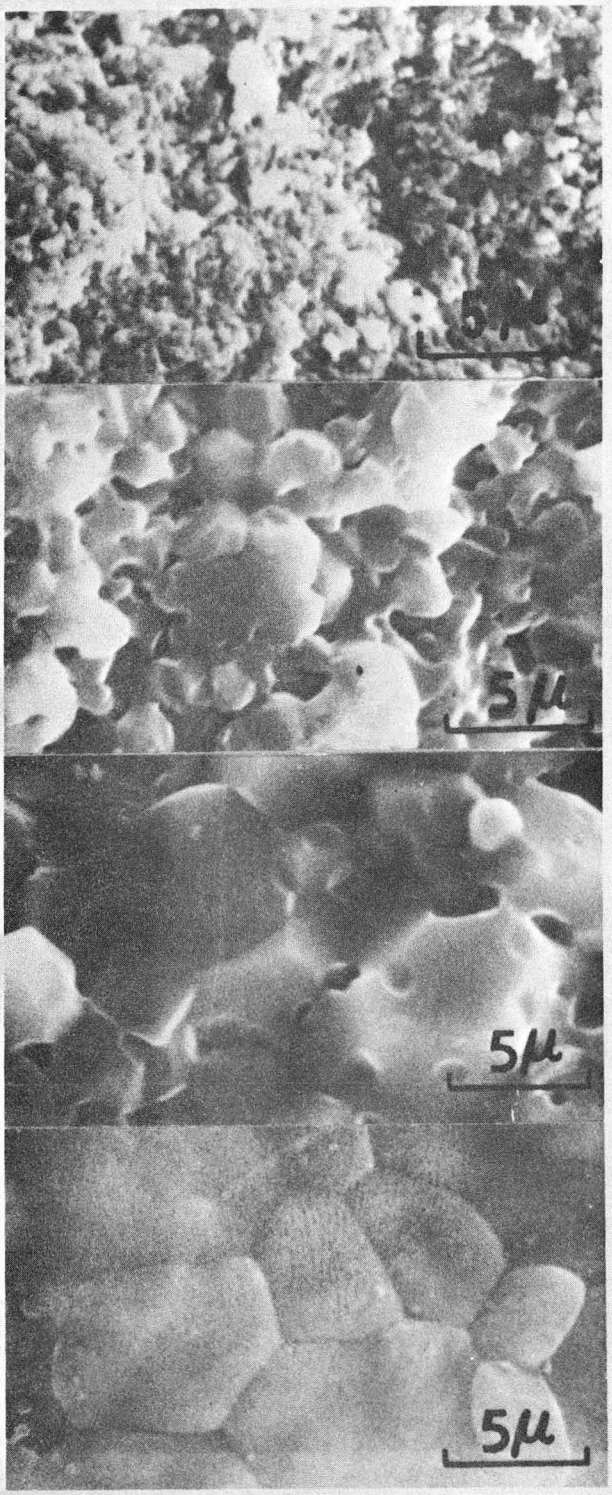

XBB780-14321

Fig. 2

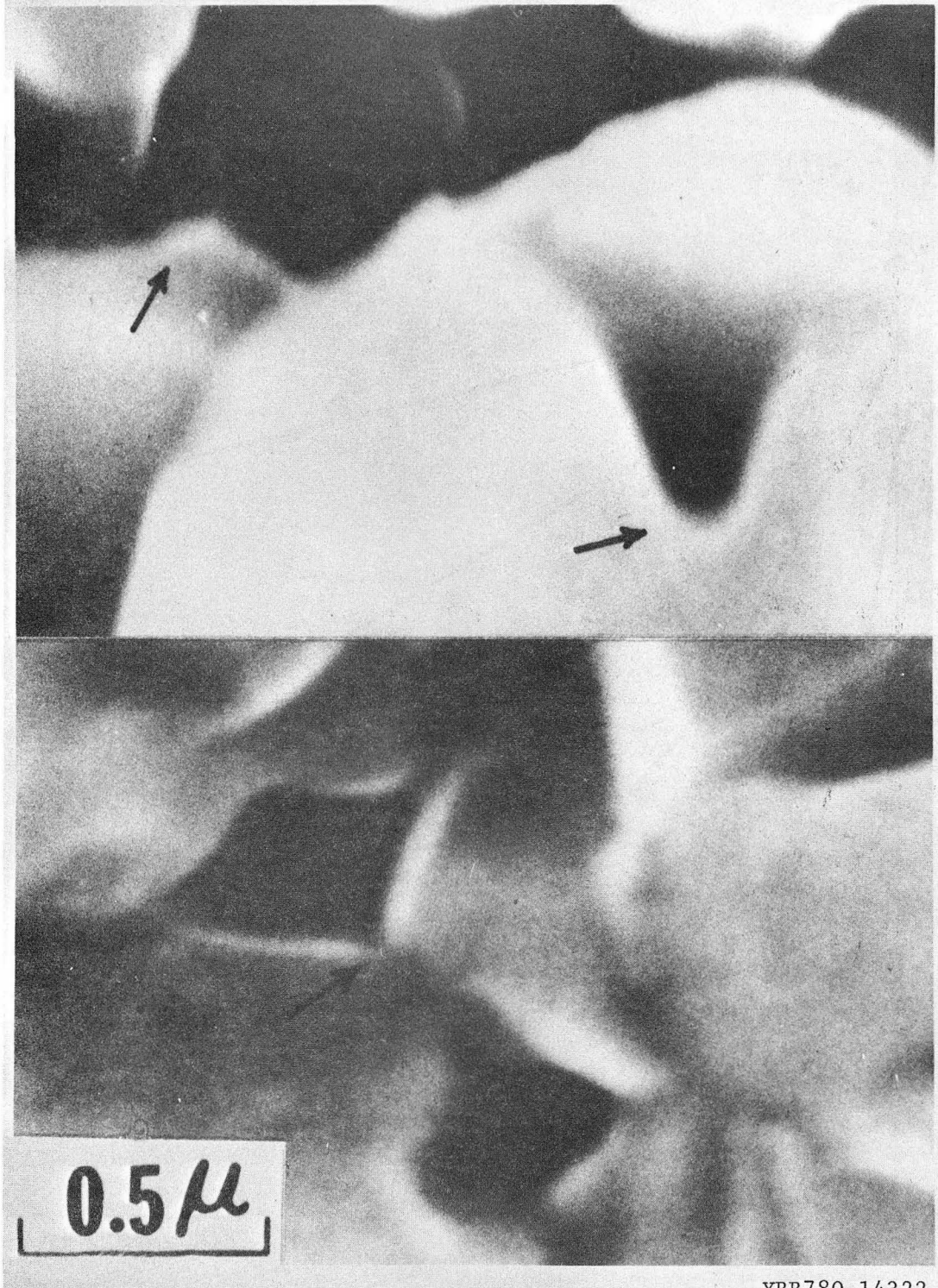

XBB780-14322

Fig. 3

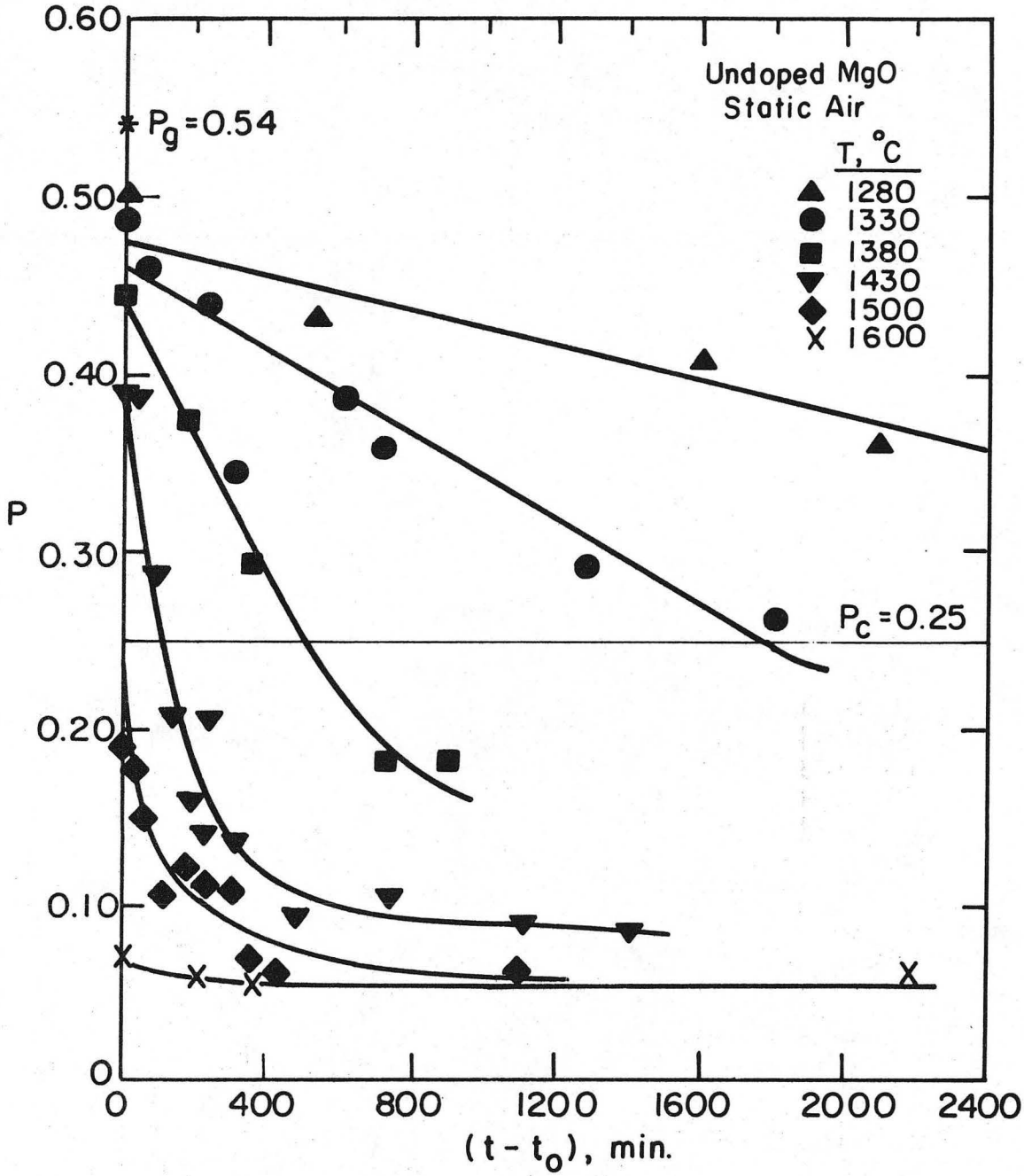

XBL 768-7410

Fig. 4

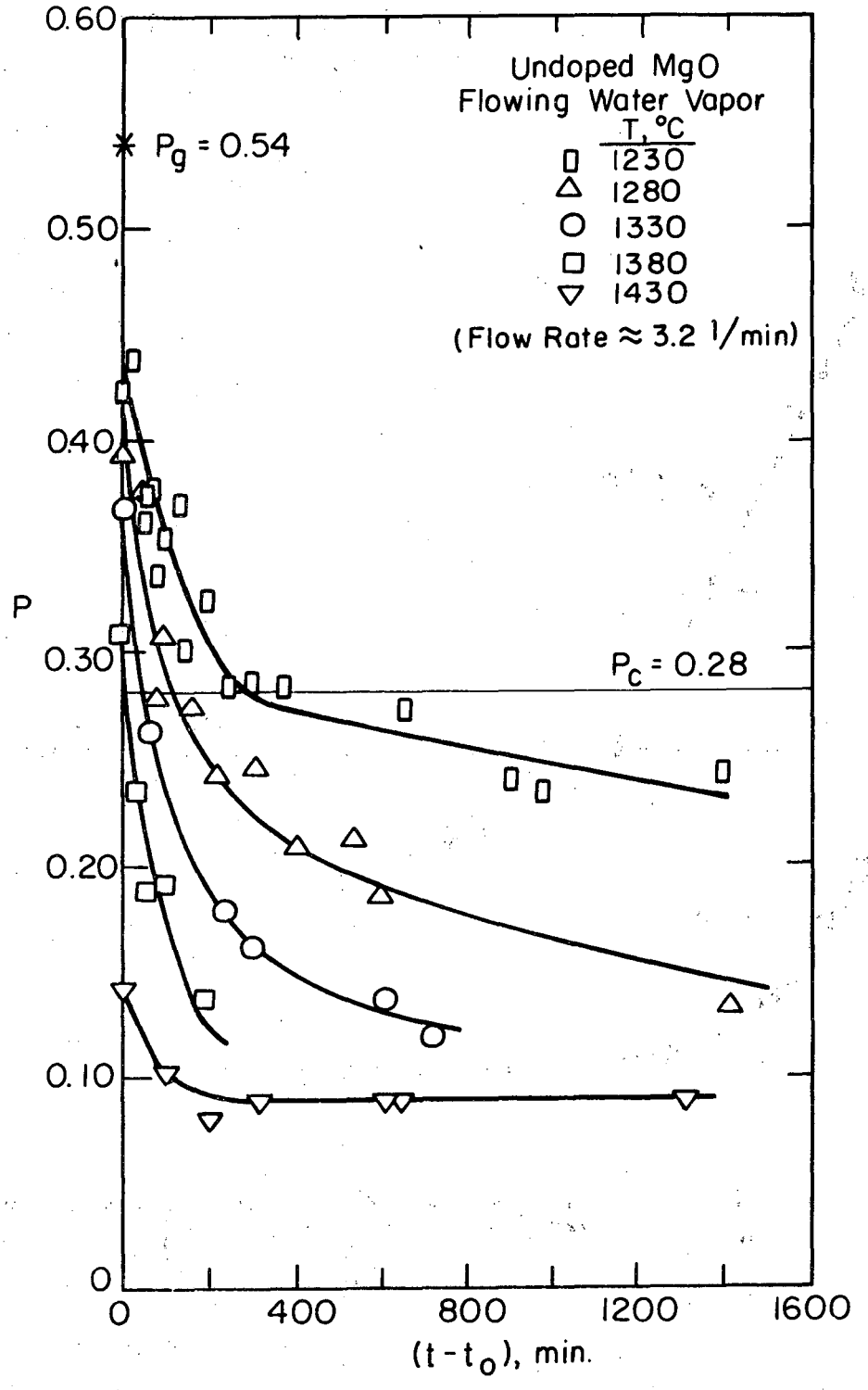

Fig. 5

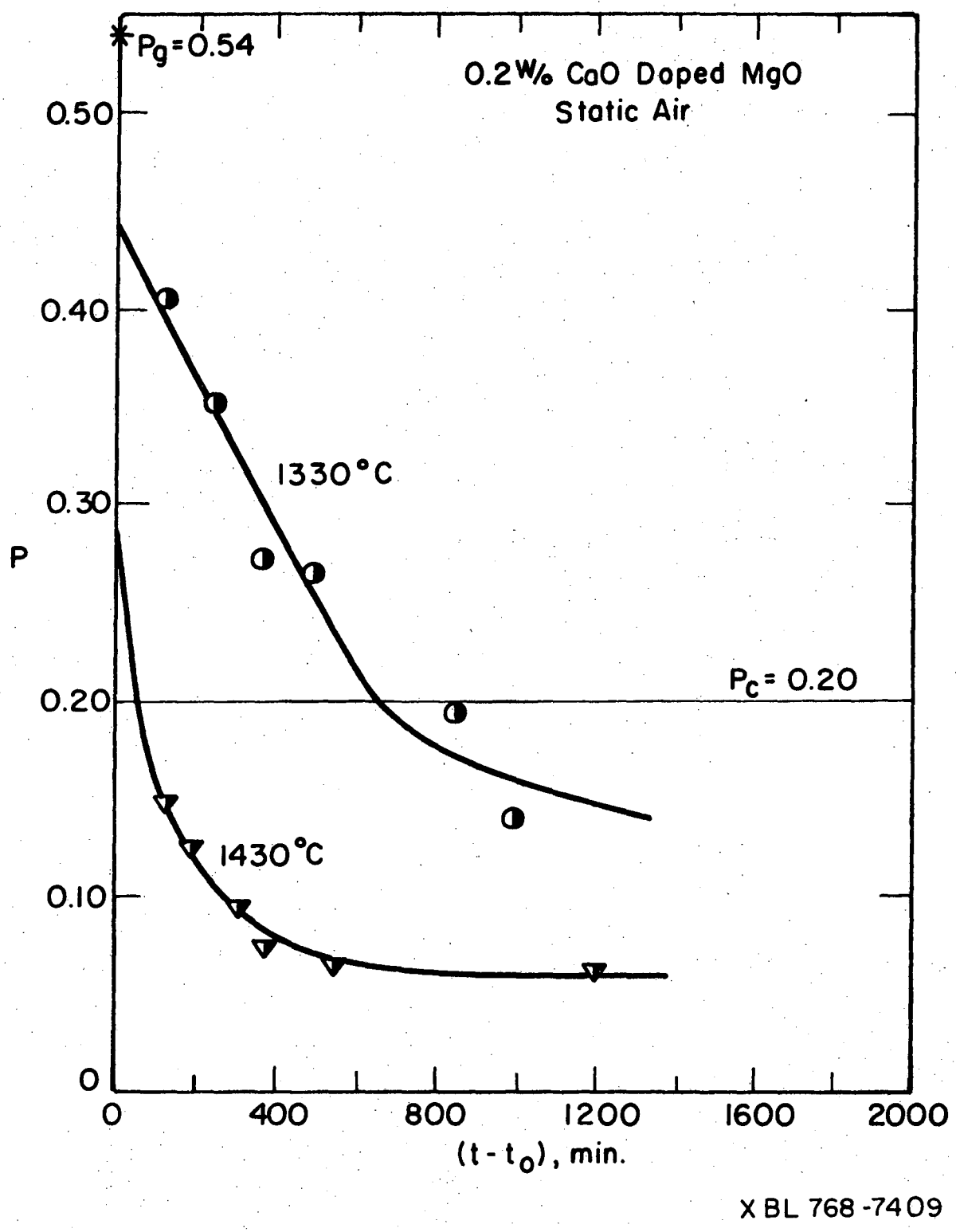
*Pg=0.54
0.2W% CaO Doped MgO
Static Air
0.50
0.40
0.30
0.20
0.10
0
P
1330°C
1430°C
Pc= 0.20
0
400
800
1200
1600
2000
(t - t0), min.
X BL 768-7409

Fig. 7

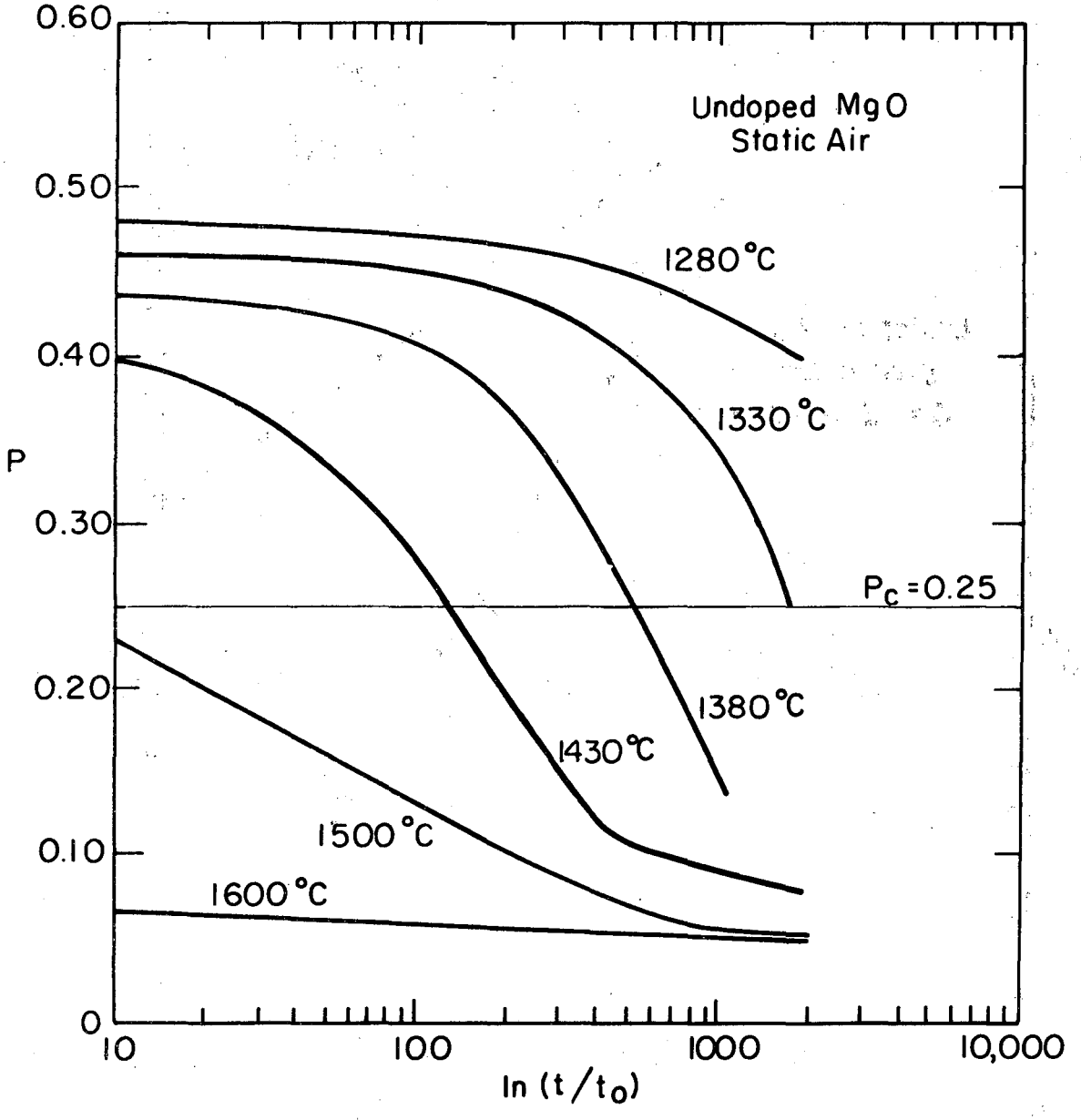

XBL 768-7416

Fig. 7

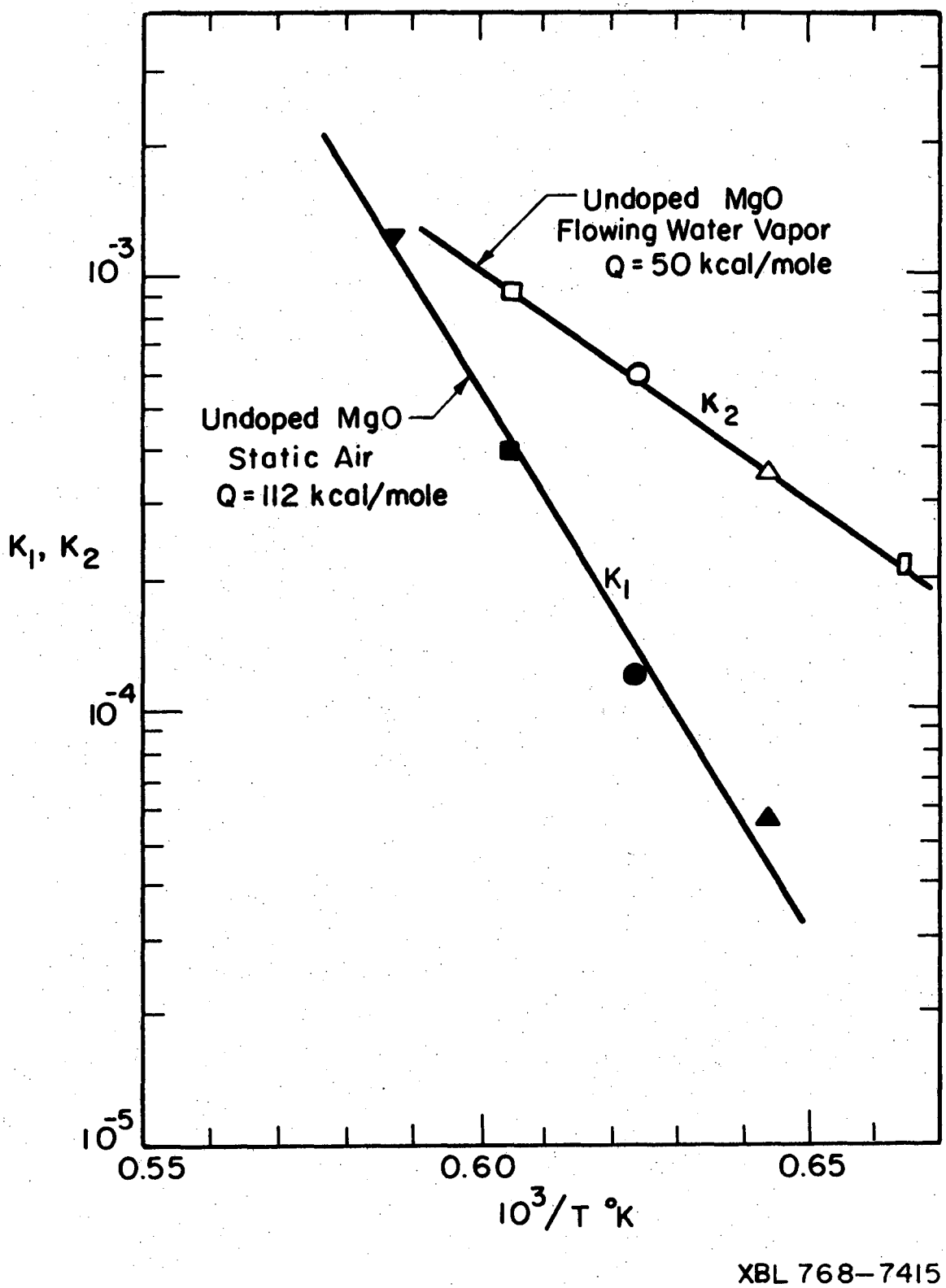
Undoped MgO
Flowing Water Vapor
Q = 50 kcal/mole
Undoped MgO
Static Air
Q = 112 kcal/mole
K2
K1
K1, K2
10-3
10-4
10-5
0.55
0.60
0.65
10³/T °K
XBL 768-7415

Fig. 8

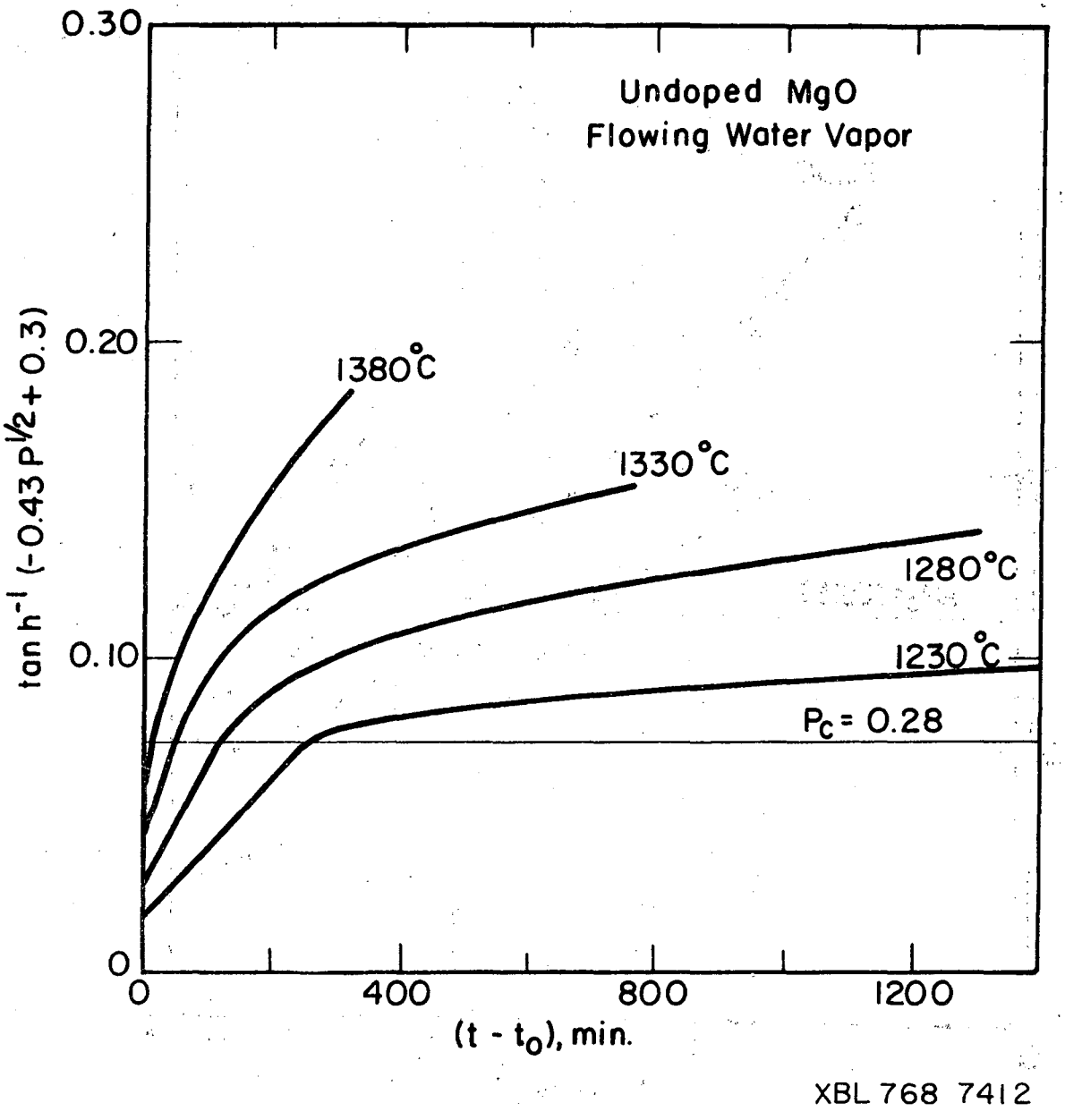

Fig. 9

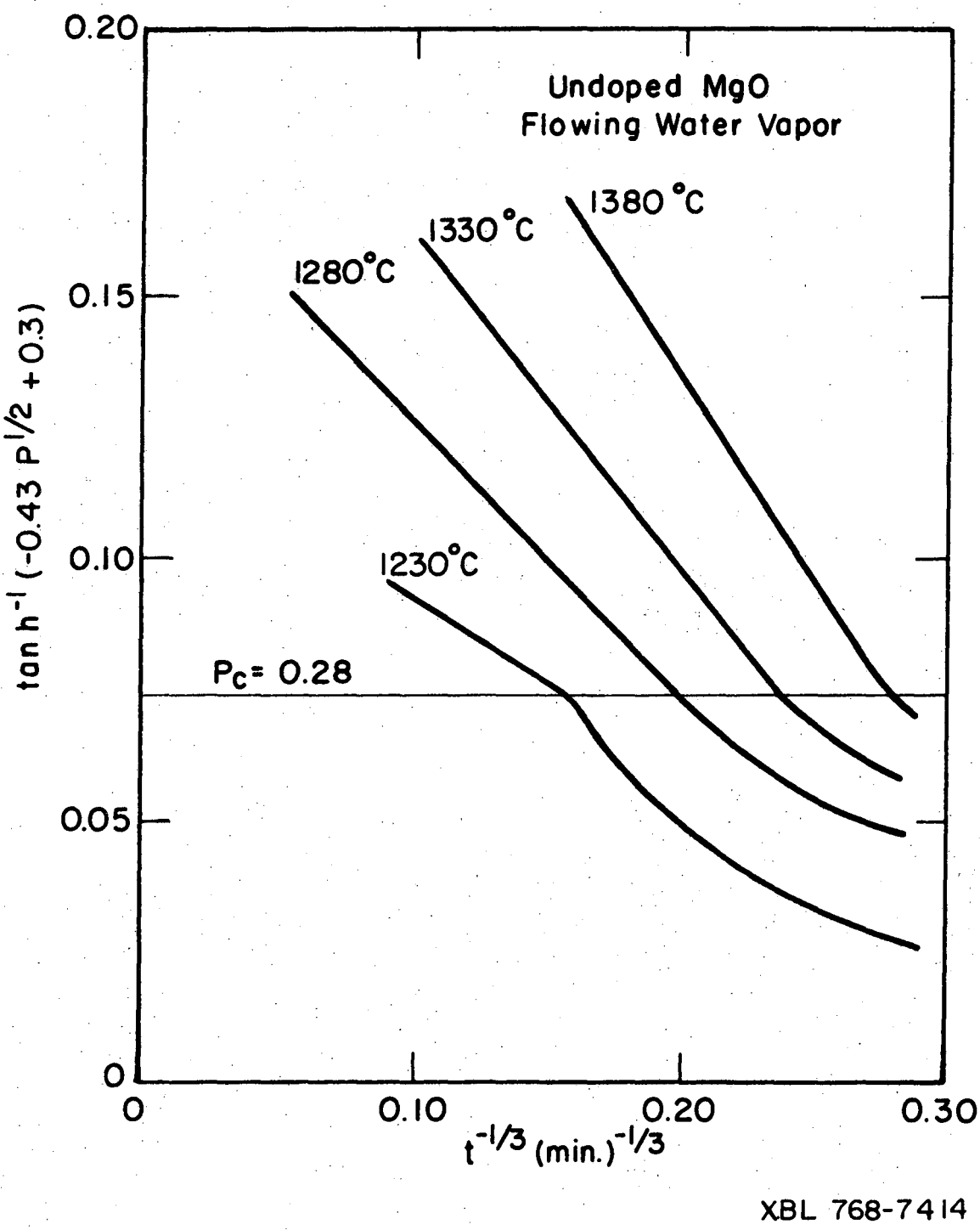
Undoped MgO
Flowing Water Vapor
1380 °C
1330 °C
1280°C
1230°C
Pc= 0.28
0.20
0.15
0.10
0.05
0
0
0.10
0.20
0.30
tan h⁻¹ (-0.43 P^1/2 + 0.3)
t^-1/3 (min.)^-1/3
XBL 768-7414

Fig. 10

TECHNICAL INFORMATION DEPARTMENT
LAWRENCE BERKELEY LABORATORY
UNIVERSITY OF CALIFORNIA
BERKELEY, CALIFORNIA 94720